Magnetic ground state of La$_2$LiMoO$_6$: A comparison with other Mo^{5+} ($S = 1/2$) double perovskites

Mirela Dragomir [●],[1,2] Adam A. Aczel [●],[3,4] Christopher R. Wiebe [●],[5,6] Joey A. Lussier [●],[5]
Paul Dube [●],[1] and John E. Greedan [●][1,7]

[1]*Brockhouse Institute for Materials Research, McMaster University, Hamilton, Ontario L8S 4M1, Canada*
[2]*Electronic Ceramics Department, Jožef Stefan Institute, Ljubljana 1000, Slovenia*
[3]*Neutron Scattering Division, Oak Ridge National Laboratory, Oak Ridge, Tennessee 37831, USA*
[4]*Department of Physics and Astronomy, University of Tennessee, Knoxville, Tennessee 37996, USA*
[5]*Department of Chemistry, University of Winnipeg, Winnipeg, Manitoba R3B 2E9, Canada*
[6]*Centre for Science at Extreme Conditions, University of Edinburgh, Edinburgh, Scotland, United Kingdom*
[7]*Department of Chemistry and Chemical Biology, McMaster University, Hamilton, Ontario L8S 4M1, Canada*

La$_2$LiMoO$_6$ is a double perovskite (DP) with $P2_1/n$ symmetry based on the Mo^{5+} ion, $4d^1$, t_{2g}^1, $S = 1/2$. It is isostructural with Sr$_2$YMoO$_6$, the magnetic ground state of which is apparently a very unusual collective spin singlet or valence-bond glass state as is the case for cubic (Fm-$3m$) Ba$_2$YMoO$_6$. Initial studies of La$_2$LiMoO$_6$ suggested a different ground state from the other DPs but no clear conclusions could be drawn. A more detailed study is presented here including magnetic susceptibility, heat capacity, and elastic neutron-scattering results. This DP is now well characterized as an antiferromagnet, $T_N = 18$ K, via observation of magnetic Bragg peaks in neutron scattering and an anomaly in the magnetic heat capacity. The ordering wave vector is $\boldsymbol{k} = (^1/_2\ ^1/_2\ 0)$, consistent with a type I face-centered-cubic magnetic structure, and the ordered moment on Mo^{5+} is $0.32(11)\,\mu_B$, much reduced from the spin-only value of $1\,\mu_B$. The index, $f = |\vartheta_c|/T_N \sim 3$, indicates a low level of frustration. The heat-capacity data above T_N can be interpreted in terms of a one-dimensional spin-correlation model, as can the low-temperature data which follow a T^1 power law. This is consistent with an earlier suggestion. The difference with isostructural Sr$_2$YMoO$_6$ is attributed to differences in the local distortion of the Mo–O octahedron and the resulting orbital ordering.

I. INTRODUCTION

Oxides with the composition $AA'BB'$O$_6$ and the double-perovskite (DP) structure where only the B' site is occupied by a magnetic ion have attracted much attention recently. As is well known by now, the B' ions occupy a face-centered-cubic lattice which is geometrically frustrated [1]. When the B' ion is from the $4d^n$ or $5d^n$ series where $n = 1$, i.e., a quantum $S = 1/2$ system, unusual magnetic ground states can result which are only partially understood given existing theory [2,3]. Among the puzzling examples are so-called doppelgänger pairs such as cubic (Fm-$3m$) Ba$_2$LiOsO$_6$ (Os^{7+}, $5d^1$) and Ba$_2$MgReO$_6$ (Re^{6+}, $5d^1$) which differ in unit cell constant by only 0.12% and, yet, the former orders antiferromagnetically below 8 K while the latter is a ferromagnet with $T_c = 9$ K [4–6]. The most bizarre example among the cubic phases is surely Ba$_2$YMoO$_6$ (Mo^{5+}, $4d^1$) which exhibits a gapped, collective singlet ground state [7–9]. This is not among the ground states found by Chen *et al.* in their mean-field analysis of cubic d^1 DP materials with strong spin-orbit coupling [2]. Even Ba$_2$YMoO$_6$ has a doppelgänger, Ba$_2$Y$_{2/3}$ReO$_6$ (Re^{6+}, $5d^1$), with a cell constant difference of 0.52%. The latter is a spin glass, $T_g = 16$ K [6].

Among DPs with monoclinic symmetry, $P2_1/n$, there are two reasonably well-characterized structural doppelgängers, Sr$_2$CaReO$_6$ and Sr$_2$YMoO$_6$, with an 0.88% difference in cell volume and very different ground states. Sr$_2$CaReO$_6$ is a

highly frustrated, unconventional spin glass with $T_g = 14$ K [10] and Sr$_2$YMoO$_6$ is reported to retain the gapped, collective singlet state of the cubic Ba$_2$YMoO$_6$ phase [11]. A search for Ca/Re site disorder using neutron pair-distribution function data yielded a null result and the origin of the spin frozen ground state is still unclear [12]. A third case involving Mo^{5+} exists, La$_2$LiMoO$_6$, also with $P2_1/n$ symmetry [7]. This material has been studied previously but its magnetic ground state has not been determined definitively. Two heat-capacity anomalies were found at ∼17 and 5 K but no lattice match was measured and the magnetic component was not isolated. Neutron-diffraction data showed no magnetic Bragg peaks but muon spin-relaxation data suggested magnetic order at least on some length scale. In this study the magnetic susceptibility has been revisited and a much more detailed set of heat-capacity data were measured along with elastic neutron-scattering data. The results of these new measurements now provide a definitive picture of the ground state of this material along with insight into the nature of the short-range spin correlations.

II. EXPERIMENTAL METHODS

A. Sample preparation

1. La$_2$LiMoO$_6$

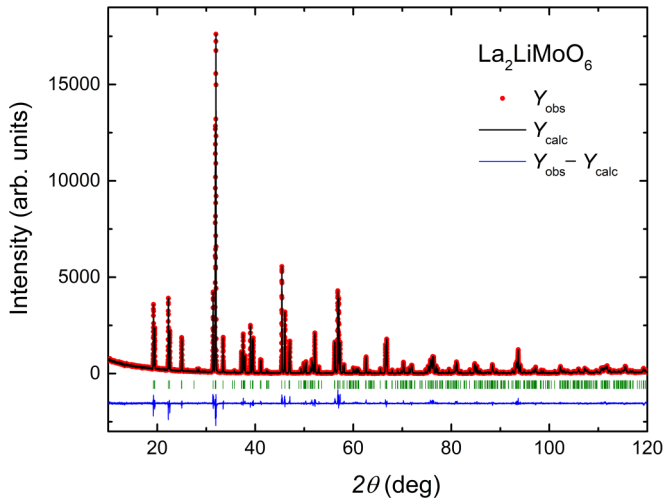La$_2$LiMoO$_6$ was prepared from La$_2$O$_3$ (99.999%, Alfa Aesar), Li$_2$MoO$_4$ (99%, Alfa Aesar), and MoO$_2$ (99.9%, Alfa

FIG. 1. A Rietveld refinement of La_2LiMoO_6. The red circles are the data, the black line the refined profile, the green tick marks locate the Bragg peaks, and the difference plot is shown below.

Aesar). The La_2O_3 was prefired at $1000\,°C$ to remove any chemical or physical water. A stoichiometric mixture of these oxides was homogenized dry in a planetary mill and then immediately pressed into rods. The rods were placed into molybdenum crucibles of about 14 cm length and with a diameter of about 1.5 cm and sealed by welding in an arc melter. The sealed Mo crucibles were then placed into a tube furnace and fired at $1100\,°C$ for 48 h, with a heating rate of $100°/h$, under Ar atmosphere. The chemical reaction that led to the formation of La_2LiMoO_6 can be written as [Eq. (1)]:

$$La_2O_{3(s)} + 0.5\,Li_2MoO_{4(s)} + 0.5\,MoO_{2(s)} \rightarrow La_2LiMoO_{6(s)}.$$
(1)
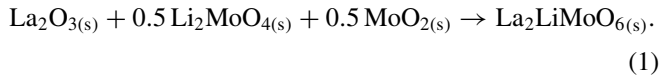
2. La_2LiNbO_6

Due to the apparent volatility of Li_2O at typical firing temperatures, the synthesis of this material was carried out by reaction of $LiNbO_3$ and La_2O_3. The mixed reactants were stored for a few weeks in air by which time the La_2O_3 had been converted to $La(OH)_3$. The firing schedule was $1100\,°C$ for 24 h followed by $1300\,°C$ for 48 h in air. This resulted in a three-phase mixture with 91% La_2LiNbO_6 and the remainder equal molar amounts of $LaNbO_4$ and La_3NbO_7, Supplemental Material, SM Fig. 1(a) [13]. Addition of an appropriate amount of $Li_2(CO_3)$ to this sample and repeating the firing schedule resulted in a product which was 99% by weight La_2LiNbO_6, [SM Fig. 1(b)]. The refined cell constants are $a = 5.614\,35(5)$ Å, $b = 5.770\,94(5)$ Å, $c = 7.937\,24(5)$ Å and $\beta = 92.2926(6)$ deg, in excellent agreement with the literature values. [14] This sample was used for heat capacity measurements.

B. X-ray powder diffraction

Laboratory x-ray diffraction data were collected with a PANalytical X-Pert Pro diffractometer with Cu-Kα_1 radiation, $\lambda = 1.540\,56$ Å, and an X'Celerator detector with a step of $0.0167°$ and a counting time of 100 s per step. Phase analysis

and structural refinements were performed with the FULLPROF program suite. [15]

C. Magnetic susceptibility

The magnetic susceptibility measurements were performed using a Quantum Design Magnetic Property Measurement System superconducting quantum interference device magnetometer. The direct current (dc) zero-field cooled (ZFC) and field-cooled (FC) data were collected in the temperature range 2–400 K under an applied magnetic field of 100 Oe. The samples were contained in gelatin capsules held in plastic straws. Empty gelatin capsules mounted above and below the samples helped to reduce the background signal. Hysteresis measurements were performed at 2, 5, and 25 K with an applied field range of $\pm 50\,000$ Oe.

D. Heat capacity

Heat-capacity data were collected on an approximately 7 mg pellet adhered to an eight-wire sapphire platform sample stage of a Quantum Design Dynacool Physical Property Measurement System heat-capacity puck using Apiezon N grease. Data were collected in zero applied magnetic field using the quasiadiabatic technique from 1.9 to 50 K. The heat capacity of the puck and grease were subtracted from the total heat capacity. Heat-capacity data collected on La_2LiNbO_6 under the same conditions were used to subtract the lattice contribution and extract the magnetic component of the heat capacity for La_2LiMoO_6.

E. Neutron scattering

Elastic neutron-scattering measurements were performed on the 14.5-meV fixed-incident-energy triple-axis spectrometer HB-1A of the High Flux Isotope Reactor at Oak Ridge National Laboratory using ~ 10 g of polycrystalline La_2LiMoO_6. The background was minimized by loading the sample in a cylindrical Al can, employing a double-bounce monochromator system, mounting two highly oriented pyrolytic graphite (PG) filters in the incident beam to remove higher-order wavelength contamination, and placing a PG crystal analyzer array before the single He-3 detector for energy discrimination. A collimation of 40'-40'-40'-80' resulted in an energy resolution at the elastic line just over 1 meV (full width at half maximum). The elastic scattering was measured between 1.5 and 100 K by loading the sample in a cryostat.

III. RESULTS AND DISCUSSION

A. X-ray powder diffraction

The results of a Rietveld refinement of data for La_2LiMoO_6 are shown in Fig. 1 and Table I. There is a weak feature not accounted for by the model at ~ 27.5 deg. which can be assigned to La_3MoO_7 and a two-phase refinement yields 1.2 wt.%. This phase has no magnetic transitions below 300 K [16]. These results are in excellent agreement with those of the previous study [7].

TABLE I. Refinement results for La$_2$LiMoO$_6$. $P2_1/n$; $a = 5.59394(3)$ Å, $b = 5.69504(3)$ Å, $c = 7.87741(4)$ Å, $\beta = 90.2634(4)$ deg. $\chi^2 = 1.54$, $R_{wp} = 8.6\%$. B_{iso} (Å^2) = 0.30.

Atom	x	y	z
La	0.9907(1)	0.0508(1)	0.2514(1)
Li	0.5	0.0	0.0
Mo	0.5	0.0	0.5
O1	0.2024(1)	0.2030(1)	0.9556(9)
O2	0.2913(1)	0.7028(1)	0.9578(8)
O3	0.0872(1)	0.4831(9)	0.2451(7)

B. Magnetic susceptibility

As this is a different sample than reported previously, it is important to establish that the bulk magnetic properties are comparable. The results of magnetic measurements are shown in Fig. 2. The Curie-Weiss fitting constants derived from Fig. 2(a) are $C = 0.283(2)$ emu K/mole Oe, $\mu_{eff} = 1.505(6)\mu_B$ and $\vartheta_c = -59(2)$ K. The fitting range was 270–400 K. These values are in excellent agreement with those obtained previously, although ϑ_c is slightly larger [7]. As well, the ZFC/FC divergence near 17 K and the broad maximum near 5 K seen in the previous sample are evident here at very similar temperatures.

C. Heat capacity

Results for both La$_2$LiMoO$_6$ and the lattice match La$_2$LiNbO$_6$ are shown in Fig. 3(a). The data for La$_2$LiNbO$_6$ were fit to a power law of the form $\beta T^3 + \gamma T^5 + \delta T^7$, with $\beta = 6.5 \times 10^{-4}$, $\gamma = -2.52 \times 10^{-7}$, and $\delta = 3.76 \times 10^{-11}$, before subtraction to obtain the magnetic contribution [Fig. 3(b)]. Note two features, a broad maximum near $\sim$28 K and a somewhat sharper maximum at $\sim$18 K which corresponds to the ZFC/FC divergence in the susceptibility
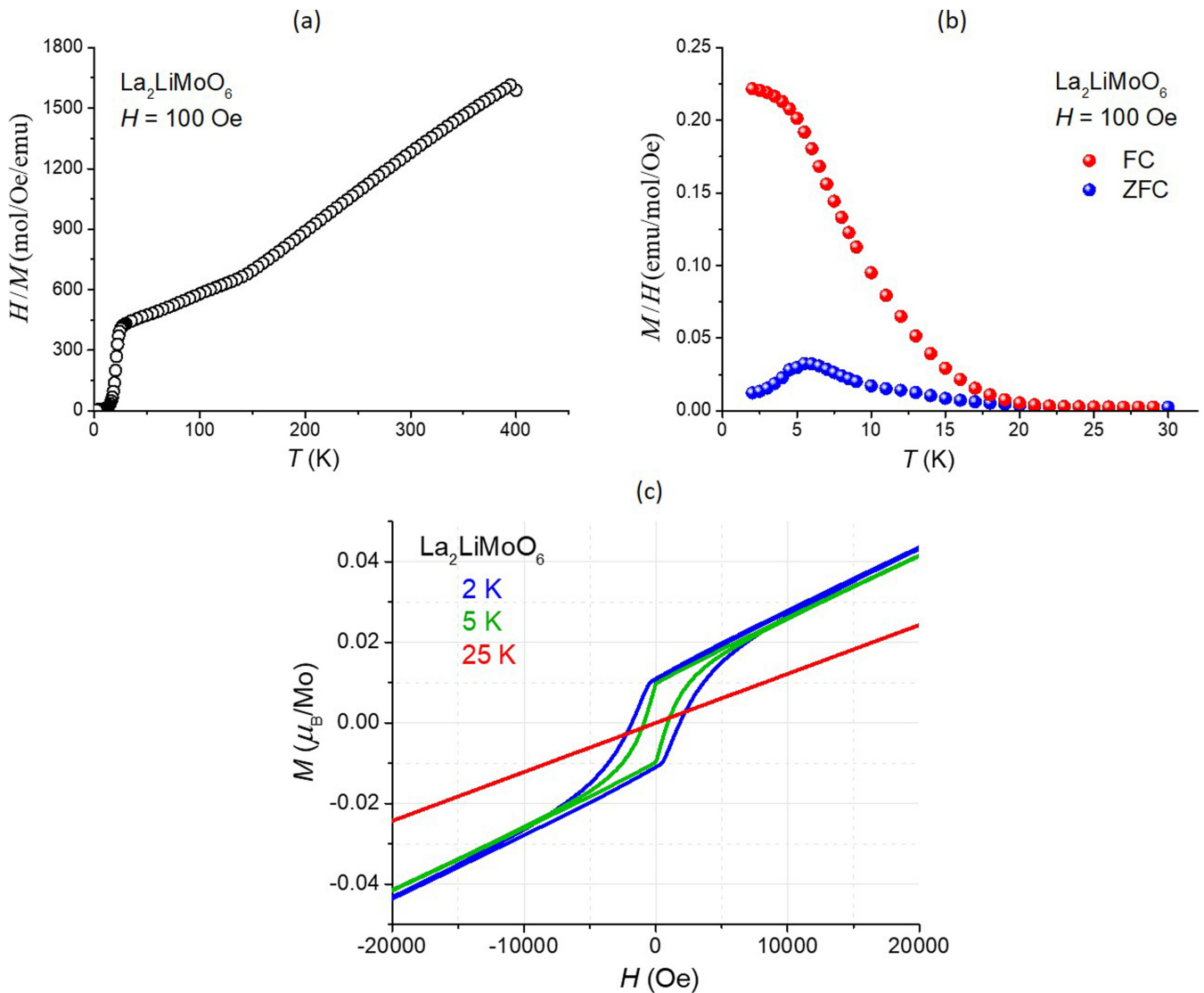

FIG. 2. La$_2$LiMoO$_6$. (a) Inverse susceptibility data. (b) Low-temperature susceptibility data, zero-field cooled (blue) and field cooled (red). (c) Magnetization data at 2, 5, and 25 K.
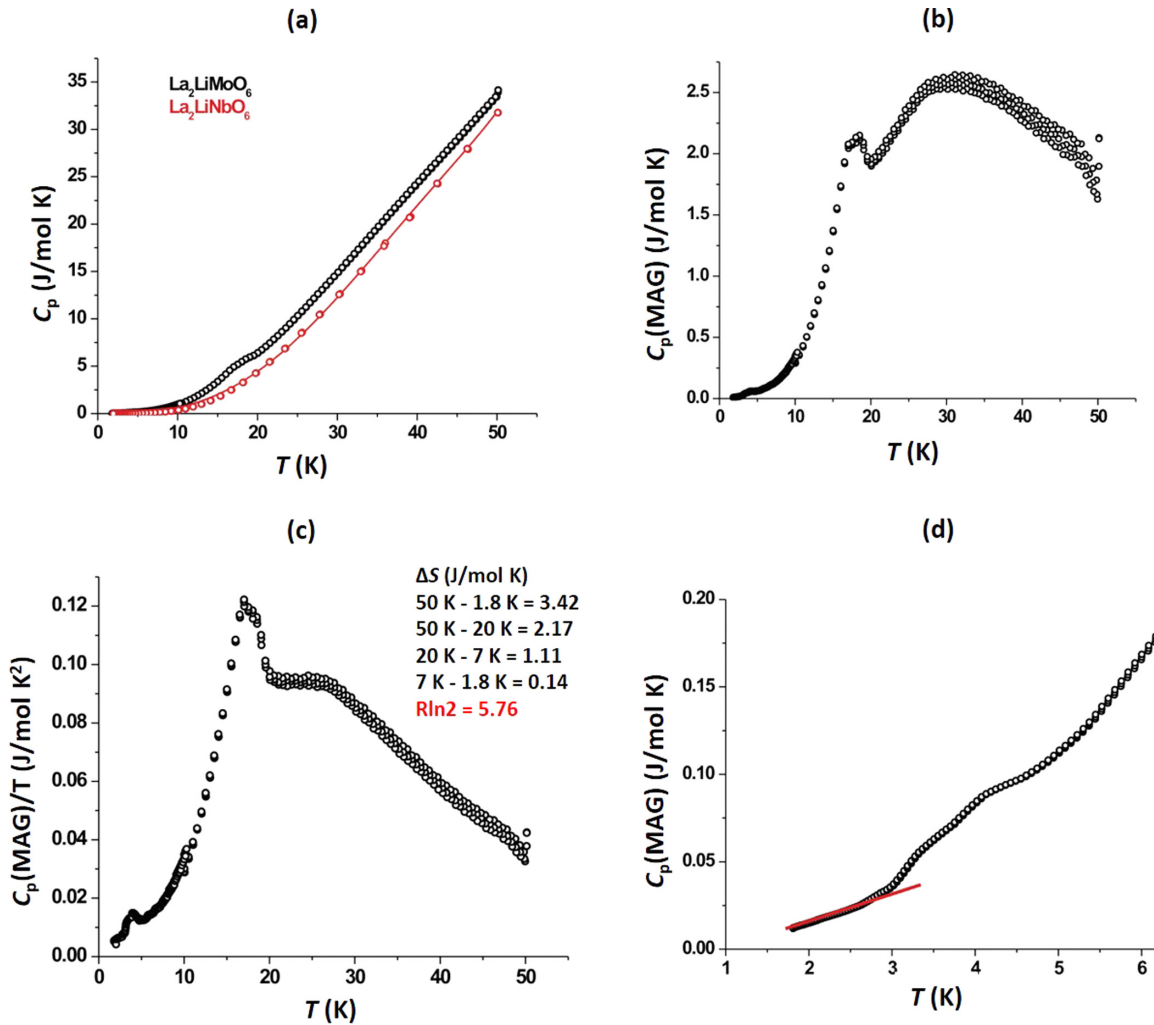
FIG. 3. Heat capacity. (a) Comparison of La_2LiMoO_6 and the lattice match La_2LiNbO_6. The red circles are the data for La_2LiNbO_6 and the solid line is the fit to the function described in the text. (b) Magnetic component for La_2LiMoO_6. (c) Entropy loss considerations. (d) Low temperature heat capacity showing a linear dependence from 1.8 to ~3 K.

[Fig. 2(b)]. Entropy loss considerations are available from Fig. 3(c). The total loss over the measured range, 1.8–50 K, is 3.42 J/mol K and approaches that for $R\ln 2 = 5.76$ J/mol K. Sixty-three percent of the entropy loss occurs between 50 and 20 K, indicating the importance of short-range spin correlations in this range. The feature at 18 K is fairly sharp, but still broad in comparison to typical lambda anomalies. The entropy loss associated with this feature (7–20 K) is 32% of the total.

The feature at ~6 K, also visible in the susceptibility data shown in Fig. 2(b), is apparent again here at a slightly lower temperature but it only accounts for 4% of the total entropy loss. The origin of this feature is unclear. It could arise from an unidentified impurity phase or it could signal a subtle spin rearrangement. Finally, at the low end of the temperature range [Fig. 3(d)], the heat capacity appears to be linear in temperature, a surprising result, as a T^3 dependence would be expected for antiferromagnetic (AF) spin waves of a three-dimensional magnet, assuming that the 18 K peak represents long-range AF order. At this stage the heat-capacity data appear to suggest short-range spin correlations over the range 50–20 K, probable long-range order below 18 K, and

an additional very weak anomaly near 6 K of unknown origin. The linear temperature dependence of C_p at the lowest temperatures is unusual.

D. Elastic neutron scattering

Data were obtained at 1.5, 10, 25, and 100 K for a wide 2θ range and selected results are displayed in Fig. 4. In Fig. 4(a) the full scattering pattern is shown out to 70 degrees; however, the magnetic information is contained in the low-angle region outlined and presented in Fig. 4(b). Note that the intensities of two peaks, marked with arrows, have a significant temperature dependence and that they are very weak. The temperature-independent peaks at ~10.5° and ~24.3° are due to unidentified impurities which were not detected in the x-ray diffraction data. Note that the second impurity peak overlaps with one of the temperature-dependent peaks. The difference (1.5–25 K) pattern shown in Fig. 4(c) clearly identifies these as magnetic peaks. The more intense peak at 16.9° was monitored with increasing temperature, as illustrated in Fig. 4(d), and it shows clear order parameter behavior with $T_N \sim 18$ K,
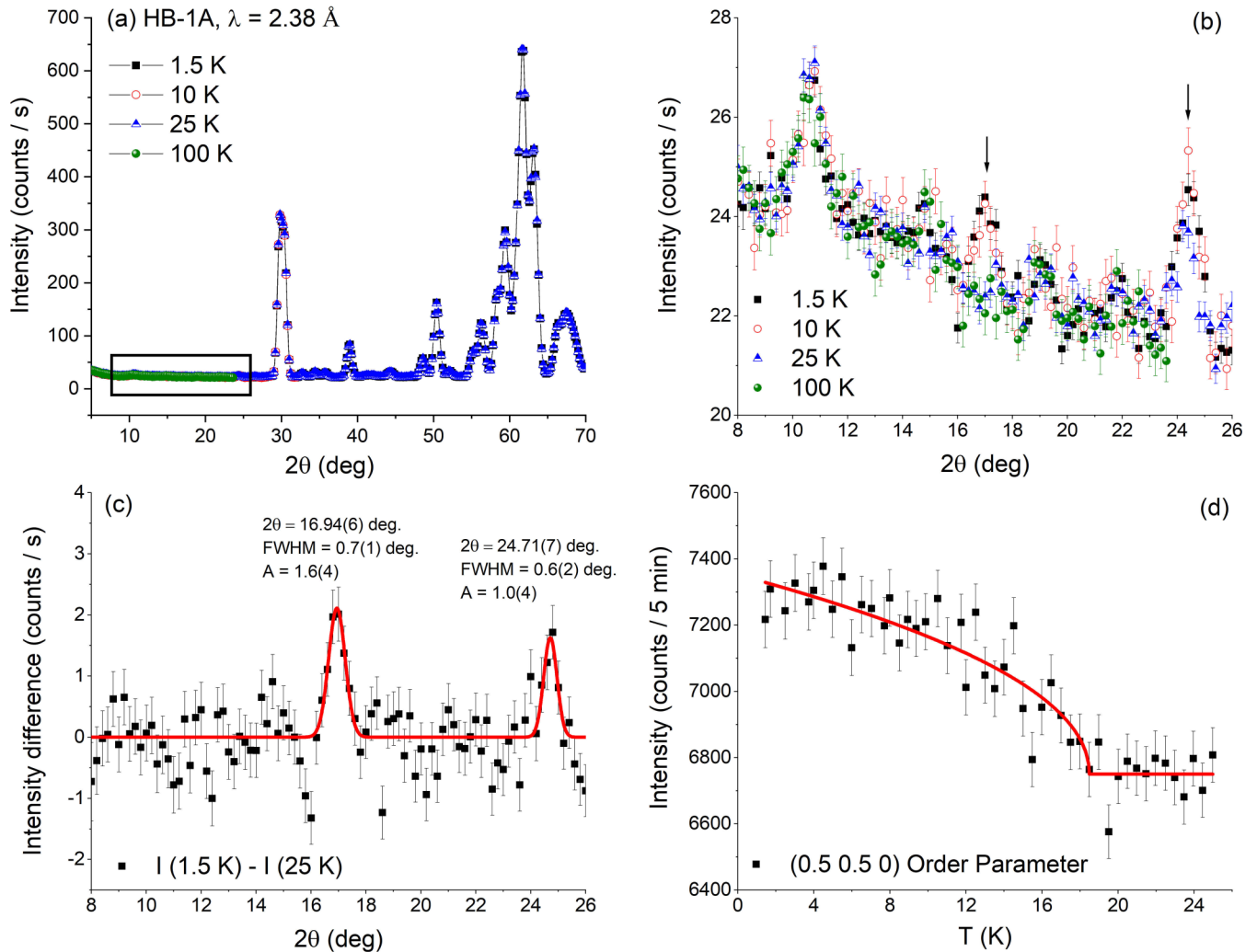
FIG. 4. (a) Elastic neutron-scattering pattern for La$_2$LiMoO$_6$, HB-1A, $\lambda = 2.38$ Å at 1.5, 10, 25, and 100 K. (b) Low-angle region showing two magnetic reflections marked by arrows. (c) Difference plot, 1.5–25 K showing the two magnetic reflections. (d) Peak intensity of the lower-angle magnetic peak, 16.9°, versus temperature indicating $T_N \sim 18$ K. The solid line is a power-law fit as described in the text.

in excellent agreement with both the susceptibility and heat-capacity data. The solid red line is a fit to a power law of the standard form: [Eq. (2)]

$$I(\mathrm{mag}) = I(\mathrm{mag})_0 (T_N - T)/(T_N)^{2\beta}. \qquad (2)$$

The variables T_N and β varied with the choice of fitting range. The fit in Fig. 4(d) covers the full range and yields $T_N = 18.5(5)$ K and $\beta = 0.24(3)$ while for the range beginning at 10 K the values become $T_N = 19.5(1.5)$ K and $\beta = 0.4(2)$. Given the large error bars in the data it is problematic to assign significance to these β values. The widths of the magnetic peaks and impurity peaks are nearly identical in a similar 2θ range, indicating that the former arises from long-range magnetic order.

The indexation of the magnetic peaks is shown in Table II. Two possible ordering wave vectors, $\boldsymbol{k} = (000)$ and $\boldsymbol{k} = (\frac{1}{2}\,\frac{1}{2}\,0)$, commonly found for monoclinic DP antiferromagnets such as La$_2$LiRuO$_6$ and La$_2$LiOsO$_6$, [17,18] were tried and clearly the latter fits the data very well.

Both wave vectors describe a type I fcc magnetic structure. From Figs. 4(a) and 4(b), the ordered moment on Mo^{5+} is very small. The moment magnitude was estimated using two approaches. First, a conventional Rietveld refinement was carried out with some significant constraints. As one of the magnetic peaks is strongly overlapped by an impurity

TABLE II. Indexation of the magnetic reflections for La$_2$LiMoO$_6$.

hkl	2θ calc. (deg)	2θ obs. (deg)
	$\boldsymbol{k} = (000)$	
001	17.709	16.95(5)
110	24.594	24.64(9)
	$\boldsymbol{k} = (\frac{1}{2}\,\frac{1}{2}\,0)$	
$\frac{1}{2}\,\frac{1}{2}\,0$	17.050	16.95(5)
$-\frac{1}{2}\,\frac{1}{2}\,1$	24.636	24.64(9)
$\frac{1}{2}\,\frac{1}{2}\,1$	24.728	24.64(9)

TABLE III. Refined structural parameters and agreement indices for La$_2$LiMoO$_6$ at 1.5 K for the HB-1A data. $a = 5.598(2)$ Å, $b = 5.772(2)$ Å, $c = 7.762(4)$ Å, $\beta = 90.49(2)$ deg, $B_{\rm iso} = 1.2(7)$ Å^2.

atom	x	y	z
La	$-0.018(2)$	$0.051(2)$	$0.247(1)$
Li	0.5	0.0	0.0
Mo	0.5	0.0	0.5
O1	$0.195(2)$	$0.220(2)$	$-0.049(1)$
O2	$0.286(2)$	$-0.306(2)$	$-0.038(2)$
O3	$0.084(2)$	$-0.523(1)$	$0.248(2)$

$R_{\rm wp} = 6.80\%$, $R_{\rm exp} = 0.94\%$, $\chi^2 = 52.2$, $R_{\rm B} = 4.01$, $R_{\rm F} = 2.49\%$.

peak, it will not be possible to determine the moment direction. Two simulations were done, one with the moment only along c ($M_x = M_y = 0$) and one with equi-axial components ($M_x = M_y = M_z$). In the first case the calculated ratio I($^1\!/_2$ $^1\!/_2$ 0)/I($^1\!/_2$ $^1\!/_2$ 1) $= 3$ and for the second case this ratio $= 1.3$, much closer to the experimental ratio $= 1.6$ derived from Fig. 4(c). Thus, the model assumes equal values for the x, y, and z components of the Mo^{5+} moment. Continuing with the Rietveld approach, a refinement including only the profile and structural variables was carried out on the 1.5 K data excluding the magnetic peak and the results are given in Table III. While the χ^2 value seems large, the structural agreement indices $R_{\rm B}$ and $R_{\rm F}$ are quite reasonable. Then, a second refinement in which these parameters were held constant and only the scale factor, background and Mo^{5+} moment were varied was performed. This result is shown in Fig. 5. The refinement converged to a total Mo^{5+} moment $= 0.32(11)\,\mu_{\rm B}$.

In the second approach the fitted area of the stronger magnetic reflection, ($^1\!/_2$ $^1\!/_2$ 0) is compared to that for a structural peak (002) which is well fit by the structural model and is of similar intensity. The observed ratio is I($^1\!/_2$ $^1\!/_2$ 0)/I(002) $= 0.23(6)$. In Fig. 6 this ratio is compared to calculated ratios for a set of Mo^{5+} moments. A value of $0.36(5)\,\mu_{\rm B}$ is obtained, very similar to and well within the error of the Rietveld refinement result.

It is of interest to compare this result with other t_{2g}^1 ions. From the $3d$ group, Ti^{3+} in the perovskite ferromagnet YTiO$_3$, has an ordered moment of $0.84(1)\,\mu_{\rm B}$ and that for V^{4+} in the ferromagnet pyrochlore Lu$_2$V$_2$O$_7$ is similar, $0.93\,\mu_{\rm B}$ [20,21]. These moments are close to the spin only value of $1\,\mu_{\rm B}$ which likely reflects the relatively small values of the spin-orbit coupling constants (SOC) and the smaller radial extent of the $3d$ orbitals relative to the $4d$ and $5d$ orbitals. Examples from the $4d$ series are sparse, there being few examples as Zr^{3+} is not stable and Nb^{4+} oxides tend to show collective rather than localized electron behavior. The present study is the only one to our knowledge in which a Mo^{5+} moment has been measured. Moments for $5d^1$ ions such as Re^{6+} and Os^{7+} are also available for ferromagnetic materials such as Ba$_2$MgReO$_6$ ($0.3\,\mu_{\rm B}$) and Ba$_2$NaOsO$_6$ ($0.2\,\mu_{\rm B}$), which are dramatically reduced from those found for $3d$ ions and close to the result for Mo^{5+} reported here [4–6] The free-ion SOC value ($\lambda = 128$ meV) for Mo^{5+} is intermediate between that for Ti^{3+} ($\lambda = 19$ meV) and the $5d$ ions Re^{6+} ($\lambda = 542$ meV)
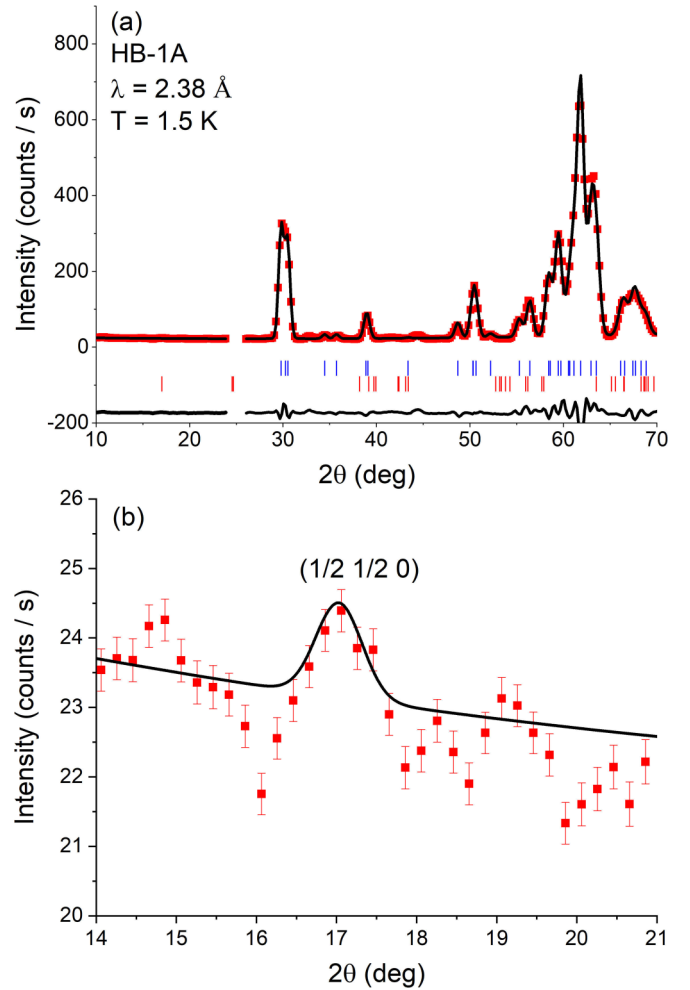

FIG. 5. (a) Rietveld fit for La$_2$LiMoO$_6$ at 1.5 K. The solid symbols are the data, the black line the fit, the blue tick marks locate the structural Bragg peaks, and the red tick marks the magnetic Bragg peaks with the difference curve at the bottom. (b) The fit to the ($^1\!/_2$ $^1\!/_2$ 0) magnetic reflection for an ordered Mo^{5+} moment of $0.32(11)\,\mu_{\rm B}$. The magnetic form factor for Os^{5+} was used in the refinement [19]. The use of other form factors such as for Cr^{3+} resulted in a moment within error of that reported here.

and Os^{7+} ($\lambda = 645$ meV) [22]. As Mo^{5+} is at the beginning of the $4d$ series, the radial extent of the $4d$ orbitals will be relatively large, and given the intermediate SOC it is likely that the reduction in moment is due more to covalency than SOC effects.

IV. SUMMARY AND CONCLUSIONS

The ground state of the monoclinic DP La$_2$LiMoO$_6$ is now well established as that of a long-range ordered AF with $T_{\rm N} = 18$ K, erasing the ambiguity from a previous report [7]. The best evidence for this comes from the observation of resolution-limited Bragg peaks of magnetic origin, supported by heat-capacity data. La$_2$LiMoO$_6$ is thus the first Mo^{5+} DP which does show long-range AF order. There are still some unconventional features, such as evidence for short-range spin correlations above $T_{\rm N}$ and an unexpected linear temperature
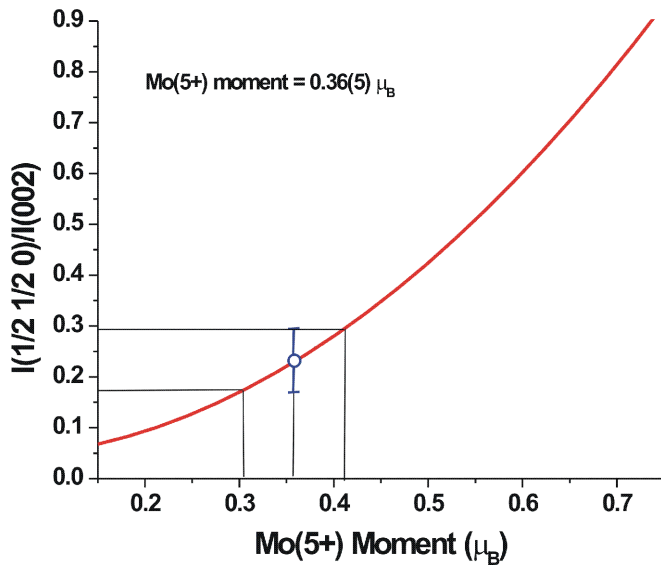
FIG. 6. Estimate of the ordered Mo^{5+} moment in La$_2$LiMoO$_6$. The red line is the calculated ratio of the intensities of the magnetic ($^1/_2$ $^1/_2$ 0) peak to the (002) structural peak. The blue circle represents the observed ratio = 0.23(6).

dependence in the low-temperature magnetic heat capacity. As well, the index, $f = |\vartheta|/T_N = 3.5$, indicates a low level of frustration [1].

All of this is in sharp contrast to the other known Mo^{5+} monoclinic DP, Sr$_2$YMoO$_6$, which has a gapped collective singlet ground state. An insight to the origin of this rather profound difference is perhaps to be found in the Mo–O coordination polyhedron in the two materials which in turn determines the nature of the orbital ordering. As shown in the previous study, the Mo–O polyhedron in La$_2$LiMoO$_6$ is well approximated by a tetragonally compressed octahedron which implies an orbital singlet $|xy\rangle$ single-ion ground

state [7]. For Sr$_2$YMoO$_6$ on the other hand, the Mo–O octahedron is tetragonally elongated which implies a ($|xz\rangle$ + $|yz\rangle$)) ground state [11]. Using a relatively simple computational approach, it was shown that for the $|xy\rangle$ case, one-dimensional spin correlations would be expected, while the ($|xz\rangle$ + $|yz\rangle$)) situation was more difficult to predict but low dimensionality is not favored [7]. It is interesting to note that the unconventional spin glass, Sr$_2$CaReO$_6$, should also have the ($|xz\rangle$ + $|yz\rangle$)) ground state [7]. There are two observations which support a one-dimensional (1D) picture for La$_2$LiMoO$_6$. First, the ratio $C_{mag}(max)/R = 0.35$ is predicted for a 1D $S = 1/2$ Heisenberg model and 0.326 for an XY model which can be compared with the observed value, 2.5 J/mole $K/R = 0.30$ from Fig. 3(b) [23]. On this basis J(1D) can also be estimated from the theoretical expression, $k_B T[C(max)]J = 0.962$ [23]. With the observed $T[C(max)] = 27.5$ K, $J(1D)/k_B = -28.6$ K. Secondly, the power law for the 1D low-temperature heat capacity can be obtained from the expression $C_p(mag) \sim T^{D/n}$ [23]. The exponent $n = 1$ for AF spin waves and thus, $C(mag) \sim T$, in agreement with the observed behavior shown in Fig. 3(d).

ACKNOWLEDGMENTS

[1] A. P. Ramirez, Strongly geometrically frustrated magnets, Ann. Rev. Mater. Sci. **24**, 453 (1994).

[2] G. Chen, R. Pereira, and L. Balents, Exotic phases induced by spin orbit coupling in ordered double perovskites., Phys. Rev. B **82**, 174440 (2010).

[3] T. Dodds, T.-P. Choy, and Y. B. Kim, Interplay between lattice distortion and spin orbit coupling in double perovskites, Phys. Rev. B **84**, 104439 (2011).

[4] K. E. Stitzer, M. D. Smith, and H.-C. zur Loye, Crystal growth of Ba$_2$MOsO$_6$ (M = Li,Na) from reactive hydroxide fluxes, Solid State Sci. **4**, 311 (2002).

[5] K. G. Bramnik, H. Ehrenburg, J. K. Dehn, and H. Fuess, Preparation, crystal structure and magnetic properties of double perovskites M_2MgReO$_6$ (M = Ca,Sr,Ba), Solid State Sci. **5**, 235 (2003).

[6] C. A. Marjerrison, C. M. Thompson, G. Sala, D. D. Maharaj, E. Kermarrec, Y. Cai, A. Hallas, T. J. S. Munsie, G. E. Granroth, R. Flacau J. E. Greedan, B. D. Gaulin, and G. M. Luke, Cubic Re (5d^1) double perovskites, Ba$_2$MgReO$_6$, Ba$_2$ZnReO$_6$ and Ba$_2$Y$_{2/3}$ReO$_6$. Magnetism, heat capacity, μSR, neutron

scattering studies and comparison with theory, Inorg. Chem. **55**, 10701 (2016).

[7] T. Aharen, J. E. Greedan, C. A. Bridges, A. A. Aczel, J. Rodriguez, G. MacDougall, G. M. Luke, T. Imai, V. Michaelis, S. Kroeker, H. Zhou, C. R. Wiebe, and L. M. D. Cranswick, Magnetic properties of the geometrically frustrated $S = 1/2$ antiferromagnets, La$_2$LiMoO$_6$ and Ba$_2$YMoO$_6$ with the B-site ordered double perovskite structure: Evidence for a collective spin singlet ground state, Phys. Rev. B **81**, 224409 (2010).

[8] M. A. de Vries, A. C. Mclaughlin, and J.-W. Bos, Valence Bond Glass on a fcc Lattice in the Double Perovskite Ba$_2$YMoO$_6$, Phys. Rev. Lett. **104**, 177202 (2010).

[9] J. P. Carlo, J. P. Clancy, T. Aharen, Z. Yamani, J. P. C. Ruff, J. J. Wagman, G. J. van Gastel, H. M. L. Noad, G. E. Granroth, J. E. Greedan, H. A. Dabkowska, and B. D. Gaulin, Singlet – triplet excitations out of the singlet ground state in the quantum fcc antiferromagnet, Ba$_2$YMoO$_6$, Phys. Rev. B **84**, 100404(R) (2011).

[10] C. R. Wiebe, J. E. Greedan, G. M. Luke, and J. S. Gardner, Spin-glass behavior in the $S = 1/2$ FCC ordered perovskite Sr_2CaReO_6, Phys. Rev B **65** 144413 (2002).

[11] A. C. Maclaughlin, M. A. de Vries, and J.-W. Bos, Persistence of the valence bond glass state in the double perovskites $Ba_{2-x}Sr_xYMoO_6$, Phys. Rev. B **82**, 094424 (2010).

[12] J. E. Greedan, S. Derahkshan, F. Ramezanipour, J. Sieweni, and Th. Proffen, Search for disorder in the spin-glass double perovskites Sr_2CaReO_6 and Sr_2MgReO_6 using neutron diffraction and neutron pair distribution function analysis, J. Phys: Condens. Matter. **23**, 164213 (2011).

[13] See Supplemental Material at http://link.aps.org/supplemental/10.1103/PhysRevMaterials.4.104406 for x-ray diffraction data for the lattice match material, La_2LiNbO_6.

[14] C. De La Torre-Gamarra, M. Woszczak, B. Levenfeld, Q. Varez, E. Garcia Gonzalez, E. Urones-Garrote, and V. Di Noto, Interplay between humidity, temperature and electrical response of a conductivity sensor based on a La_2LiNbO_6 double perovskite, J. Mater. Chem. A **6**, 5430 (2018).

[15] J. Rodríguez-Carvajal, Recent advances in magnetic structure determination by neutron powder diffraction. Phys. B (Amsterdam, Neth.) **192**, 55 (1993).

[16] H. Nishimine, M. Wakeshima, and Y. Hinatsu, Structures, magnetic and thermal properties of Ln_3MoO_7 (Ln = La, Pr, Nd, Sm and Eu), J. Solid State Chem. **178**, 1221 (2005).

[17] P. D. Battle, C. P. Grey, M. Hervieu, C. Martin, C. A. Moore, and Y. Park, Structural chemistry and magnetic properties of La_2LiRuO_6, J. Solid State Chem. **175**, 20 (2003).

[18] C. M. Thompson, C. A. Marjerrison, A. Z. Sharma, C. R. Wiebe, D. Maharaj, G. Sala, R. Flacau, A. Hallas, Y. Cai, B. D. Gaulin, G. M. Luke, and J. E. Greedan, Frustrated magnetism in the double perovskite La_2LiOsO_6. A comparison with La_2LiRuO_6, Phys Rev B **93**, 014431 (2016).

[19] K. Kobayashi, T. Nagao, and M. Ito, Radial integrals for the magnetic factor of the 5d transition elements, Acta. Crystallogr. A **67**, 473 (2011).

[20] J. D. Garrett, J. E. Greedan, and D. A. MacLean, Crystal Growth and Magnetic Anisotropy of $YTiO_3$, Mater. Res. Bull. **16**, 145 (1981).

[21] L. Soderholm and J. E. Greedan, Magnetic Properties of the Pyrochlores $(RE)_2V_2O_7$; RE = Tm, Yb, Lu. New Ferro- and Ferrimagnetic Semiconductors, in *The Rare Earths in Modern Science and Technology* (Plenum Press II, New York, 1980), pp. 393–394; G. V. Bazuev, O. V. Marakova, V. Z. Oboldin, and G. P. Shveikin, New ferromagnetic semiconductor oxides with a pyrochlore structure, Dokl. Akad. Nauk SSSR **230**, 861 (1974).

[22] C.-G. Ma and M. G. Brik, Systematic analysis of spectroscopic characteristics of heavy metal transition metal ions with $4d^N$ and $5d^N$ (N = 1 − 10) electronic configurations in a free state, J. Lumin. **145**, 402 (2014).

[23] L. J. de Jongh and A. R. Miedema, Experiments on simple model systems, Adv. Phys. **23**, 1 (1974).